Efficient and Stable Self-passivation Perovskite Solar Cells Prepared in Ambient Air based on Anti-solvent Free Method

Qiqi Zhang[a], Seid Yimer Abate[a], Guorong Ma[b], Yifang Qi[a], Jada Emodogo[a], Kira Williams[a], Shafi Muhammad[a], Zhongliang Ouyang[c], Paresh Chandra Ray[a], Glake Alton Hill Jr[a], Xiaodan Gu[b], Dawen Li[c], and Qilin Dai[a]*

[a] Department of Chemistry, Physics, and Atmospheric Sciences, Jackson State University, Jackson, MS, 39217, United States

[b] School of Polymer Science and Engineering, Center for Optoelectronic Materials and Devices, The University of Southern Mississippi, Hattiesburg, MS 39406, United States

c Department of Electrical and Computer Engineering, Center for Materials for Information Technology, The University of Alabama, Tuscaloosa, AL 35487, United States

*Corresponding author: qilin.dai@jsums.edu

Abstract: Solution processable perovskite solar cells (PSCs) are one of the most promising candidates for commercialization. However, the perovskite film preparation method is limited by the mandatory anti-solvent process under inert gas atmosphere which significantly influenced its mass production. In this study, we developed a perovskite film preparation without the requirement of anti-solvent dripping in air. We employed various solvents to prepare perovskite film and study their influence on perovskite nucleation and morphology for respective solvents. Among them the perovskite prepared using dimethylacetamide (DMAc), which has low solubility and high interaction with PbI_2, demonstrated highly crystalline perovskite black phase without anti-solvent dripping. Furthermore, we found that perovskite concentration played an important role in the perovskite film quality, where the high concentration DMAc based perovskite produced smooth and dense perovskite film by antisolvent free method in air. PSCs fabricated using this technique delivered champion power convert efficiency (PCE) of 20.1%. At the same time, the best device prepared by blade coated method also gets 18% PCE. Moreover, the unencapsulated devices exhibited excellent stability which retained more than 90% its initial efficiency after 47 days in air. This work provides a facile and cost-effective method towards a controllable fabrication of high-performance anti-solvent free $MAPbI_3$ based solar cells.

Keywords: Anti-solvent free; dimethylacetamide; thickness control; large-area perovskite film preparation.

1. Introduction

In this rapid industrial period, the photovoltaic (PV) devices provide sustainable clean energy and contributed significantly to satisfy the global energy demands and environmental concerns.[1-3] Among various solar cells, perovskite solar cells have attracted the attention of researchers and PV industries because perovskite has excellent light harvesting,[4-5] remarkable optoelectronic properties,[6-7] small exciton binding energy and superior optoelectronic properties,[8] as a result, the PSCs devices PCE swiftly increased from 3.8% to over 25% in the past decade.[9-11]

However, PSCs devices demonstrated significantly high performances the perovskite layer preparation required complicated and time accurate anti-solvent dripping by an anti-solvent to remove the excess solvent and accelerate the crystallization of perovskite.[12-13] The anti-solvent type, amount and dripping time significantly influences the perovskite crystallinity and morphology and this is one of the major obstacles to reproduce lab results.[14] Moreover, the perovskite film processed in N_2 glove box. Generally, in the ordinary PSC fabrication by one-step procedure the perovskite layers were prepared under N_2 glove box by spin coater and with anti-solvent dripping. [15-16] The traditional solvents used to prepare perovskite precursor such as N, N-Dimethylformamide (DMF), dimethyl sulfoxide (DMSO), and gamma-Butyrolactone (GBL) are required anti-solvents such as chlorobenzene, diethyl ether and ethyl acetate to achieve homogenous and crystalline black perovskite and their fabrication process carried out in N_2 glovebox.[17-20] In most cases, when the devices fabricate in air, moisture and oxygen are interfered in the fabrication process and the devices couldn't survive for long which hampers the mass production and real application of the PSCs that makes the PSCs impact limited in lab. Some efforts were discovered to improve the air fabricated perovskite stability such as doping of Rb, Cs, Br and Cl ions.[21-26] These ions interaction with the perovskite components and passivated the

uncoordinated Pb^{2+} and halide ions, however, still the PCE was lower than the perovskite prepared in N_2 condition. Therefore, it is an urgent task to develop a new perovskite fabrication pathway to fabricate perovskite film in ambient air without the need of anti-solvent.

The perovskite morphology comprises polycrystalline structure as a result there are substantial grain boundary defects. Besides adding other component in perovskite precursor to passivate the defects, using excess lead iodide (PbI_2) or methylammonium iodide (MAI) or formamidinium iodide (FAI) could self-passivate and reduce recombination losses at grain boundaries.[27-28] Regrettably, some reports demonstrated that the unbalance stoichiometric ratio in the perovskite layer is detrimental to the overall device stability.

Recently, spin coating of self-volatilization solvent-based perovskites has drawn enormous research interest to realize anti-solvent free perovskite films.[29-31] Such solvents, have low boiling point, and high vapor pressure, such as, 2-methoxyethanol (2-ME), methylamine (MA) ethanol, acetonitrile (ACN), with polar aprotic solvents perovskite prepared with such mixtures could produce high-quality perovskite film without the need of anti-solvent.[32-34] The reason is during spin coating process the self-volatilization solvents rapidly evaporate and the solution will reach supersaturation rapidly and formed nuclei. Later, the wet film will convert to the solid perovskite black phase entirely through crystal growth. Unfortunately, self-volatilization solvent-based perovskites have a common disadvantage, the nucleation rate is too quick, leading to formation of low coverage and defective perovskite film. As a result, self-volatilization solvent must mix with solvents capable of strongly interacting with perovskite precursors to form an intermediate phase and delay the rate of nucleation to achieve homogenous and compact perovskite morphology.

DMAc is a homologues solvent with DMF, as a result, DMAc can be an alternative suitable solvent to prepare perovskite precursor.[35-37] DMAc besides dissolution it could form reaction with

the PbI_2. The O atoms in DMAc could combine with Pb atoms to form covalent bond, the bonding energy is lower than Pb-O in DMF, because DMAc has a weaker polarity than DMF, the coordination between DMAc and PbI_2 is lower than that of DMF and PbI_2,[38] When CH_3NH_3I dissolved in DMAc, they connect through hydrogen bonding, it's between O-C bond ant the N-H bond, when CH_3NH_3I and PbI_2 dissolve in DMAc in the same time, the Pb-O bonds between PbI_2 and DMAc is replaced by hydrogen bonds, due to the weak interaction between PbI_2 and DMAc, supersaturation of $CH_3NH_3^+$ around the PbI_2 crystal lattice, CH_3NH_3I and PbI_2 will self-assemble to form $CH_3NH_3PbI_3$, the organic cation easily inserts into the soft Pb-I framework and promote perovskite grain growth and enhances crystallinity.[39-41] And the stabilization energy between DMAc and $CH_3NH_3PbI_3$ is smaller than it between DMF and $CH_3NH_3PbI_3$, which means $CH_3NH_3PbI_3$ is easier escape from DMAc without antisolvent.[35] Moreover, due to the interaction of DMAc and perovskite the neighboring perovskite grains crosslinked where the acetamide stayed at the grain boundaries and passivated the local shallow-level defects.[42] During spin coating process, perovskite begins to nucleate as DMAc is removed, and in the same film fabrication process, the low concentration of perovskite precursor results in low concentration of the nucleus, this will lead to low surface coverage films.[38] Therefore, the different concentration perovskite precursors to get a compact perovskite film need to be investigated.

Herein, we employed DMAc solvent to fabricate high quality anti-solvent free self-passivated perovskite film in air. We found that perovskite films prepared from high concentration perovskite in DMAc exhibited homogenous grain growth and enhanced crystallinity as a result thick and homogenous perovskite films formed. PSCs fabricated using high concentration DMAc (2.12 mM). delivered a champion PCE of 20.1% on anti-solvent free $MAPbI_3$ based device. Furthermore, we employed blade coater to fabricate large area perovskite films from the DMAc-based perovskite

precursor and an outstanding performance of 18% PCE achieved. Our results clearly suggest DMAc is a promising solvent to fabricate homogenous compact perovskite films in air and could be implemented to fabricate high large area and could be employed photovoltaic devices.

2. Experimental procedures

2.1 Materials

Fluorine-doped tin oxide (FTO)-coated glasses purchased from Advanced Election Technology Co, Ltd. The tin (IV) oxide (SnO_2), 15% in H_2O colloidal dispersion, DMAc were obtained from Alfa Aesar. 2ME, DMF, chlorobenzene (CB), acetonitrile, 2,2,7,7-tetrakis-(N, N-di-p-methoxy[henylamine]-9,9 spirobifluorene (spiro-OMeTAD, 99%) were acquired from Sigma-Aldrich, PbI_2, bi(trifluoromethane) sulfonimide lithium salt (Li-TFSI, 99%) were purchased from TCI, 4-tert-butylpyridine was obtained from Accela. FK 209 Co(III) TFSI salt and Methylamine iodide were purchased from Great Solar Australia Pty.

2.2 Devices fabrication

The FTO glass substrates were washed by detergent, DI water, acetone, and isopropyl alcohol sequentially in a sonication bath for 15 min. Then the subtracts were dried by flowing dry air and followed by 45 min UV ozone treatment. The SnO_2 aqueous colloidal dispersion was diluted with deionized water in a volume ratio of 1:3, then spin-coated on the substrates at 7000 rpm for 30s, followed by annealing at 150 ^{o}C for 30 min by a hotplate to form the compact SnO_2 films. Subsequently, the FTO/SnO_2 films were UV ozone for 5 min and different concentration perovskite precursor were spin coated on it at 6000 rpm for 30 s to form perovskite films, then

annealed at 100 °C for 30 min. The control perovskite precursor solutions were prepared by dissolving 1.06 mM MAI and 1.06 mM PbI_2 in 1 ml DMAc/2-ME/DMF as 1 times. Consecutively, we prepared 1.25 times, 1.5 times, 1.75 times, and 2 times perovskite precursor solution with a concentration of 1.325 mM, 1.59 mM, 1.855 mM, and 2.12 mM, respectively. If over 2 times, it couldn't fully dissolve to make devices. After that, the hole transport layer solution which contain 90 mg spiro-OMeTAD, 22.5 µl Li-TFSI (550 mg of Li-TFSI in 1 ml acetonitrile), 39 µl 4-tert-butypylridine and 10 µl Co(III)TFSI (375 mg Co(III) TFSI in 1 ml acetonitrile) all dissolved in 1 ml chlorobenzene was spin coated on the top of perovskite films with 4000 rpm for 30 s. Finally, a 50 nm thick Au electrode was deposited on top. The active aperture area of the devices is 0.085 cm^2 decided by the masks. For the blade coated perovskite device, the SnO_2, $MAPbI_3$, and Spiro-OMeTAD films were prepared by blade coating at a speed of 20 mm/s, 1.5 mm/s, and 2.5 mm/s, respectively. To accelerate the film drying and crystallization of perovskite film, a 40 psi N_2-flow was introduced during blading the $MAPbI_3$ layers. All the blade-coated films including SnO_2, $MAPbI_3$ and spiro-OMeTAD are blade-coated at room temperature without prewarming. All the processes were operated in air (temperature ~ 30°C, RH < 20 %).

3. Characterization

The characterization of perovskite and modified perovskite films was performed by X-ray diffraction (XRD), ultraviolet-visible (UV-Vis), scanning electron microscopy (SEM), photoluminescence (PL), time-resolved photoluminescence (TRPL), X-ray photoelectron spectroscopy (XPS), grazing-incidence wide-angle X-ray scattering (GIWAXS), electrical impedance spectra (EIS), and all I-V, external quantum efficiency (EQE) measurement were done

using the apparatus described in previous work. All the devices were characterized without encapsulation.[43-45] Dynamic light scattering (DLS) was performed on Litesizer 100.

4. Results and discussion

4.1 Precursor solvent effect on perovskite films

Nowadays, the solution processing methods are the most popular method to prepare perovskite films because of their low cost and facile fabrication.[46-48] However, to prepare the perovskite precursor solution there are limited number of solvents. The solvent must have sufficient polarity to dissolve the perovskite precursor in our case PbI_2 and MAI.[49-51] Additionally, the solvent vapor pressure, boiling point, viscosity, and related properties could influence the perovskite crystallization and morphology.[36, 52] When highly volatile solvent used the evaporation rate is too rapid and controlling the crystallization is difficult.[29] On the other hand, when non-volatile solvents employed to prepare the perovskite anti-solvent is required to achieve the required homogenous crystalline perovskite. Therefore, choice of precursor solvent plays a critical role in perovskite film formation and perovskite morphology.

In general, 2-ME is the most common solvent used to fabricate perovskite film without anti-solvent, however, perovskite precursor prepared by DMF solvent required anti-solvent. Here we employed DMAc, one of the homologue solvents of DMF to fabricate anti-solvent free perovskite layer and we critically studied the why DMAc is a suitable and promising solvent to fabricate perovskite in anti-solvent free method. First, we investigated the solubility of PbI2 in 2-ME, DMF, and DMAc solvents (1mM PbI_2 in 1mL respective solvent). The solubility tests confirmed that PbI_2 is hardly reacted with 2-ME, where the PbI_2 settles at the bottom of the vial after shaking by

high-speed vortex for 2 hours (see the inset photographs in Figure S1). Unlike 2-ME, both DMF and DMAc reacted with the PbI_2 and formed intermediates which are clearly presented in Figure S1. Second, we studied the XRD of PbI_2 in 2-ME, DMF and DMAc and compared with the standard single crystal PbI_2 (JCPDS #07-0235) where only diffraction peaks from the PbI_2 has detected without intermediate phase formation when 2-ME employed which directly supported 2-ME doesn't dissolve PbI_2. On the other hand, the PbI_2 completely dissolved in DMF, the solution color turn to yellow, and the XRD exhibited a DMF-PbI_2 intermedia phase about 2-theta (9.05 and 9.6 degree). However, the DMAc solvent is reacted with the PbI_2 and formed white precipitate not clear yellow solution like DMF. The XRD of the DMAc-PbI_2 demonstrated the formation of intermediate phase similar with DMF-PbI_2 which showed the PbI_2 is soluble in DMAc, but its solubility is lower than DMF. In order to get clearly perovskite solution, MAI been added in these vials, it will connect with PbI_2 or DMF-PbI_2 or DMAc -PbI_2 intermedia phase, the precipitate will dissolve and form colloidal perovskite in these solvents.

Figure 1 exhibited the SEM surface morphology of various concentration perovskite precursor prepared perovskite films based on 2-ME, DMF and DMAc solvents. Figure 1a-1c and Figure 1d-f displayed $MAPbI_3$ films when the concentration is 1 times and 2 times, respectively. Figure 1a showed perovskite film prepared with 2-ME perovskite precursor, where non-homogenous multi-layer and pin hole containing perovskite morphology formed. Figure 1b showed the morphology of perovskite film when DMF is employed to prepare the precursor solution in which a single layer film with rod shape structure formed, consequently, the perovskite coverage is limited where large area of the FTO exposed in the SEM monograph. Figure 1c showed the perovskite film morphology when the perovskite precursor is prepared by DMAc solvent, smaller perovskite grains formed. Unlike the DMF, the DMAc 1 times morphology demonstrated better film coverage,

however still voids are present in the film. When the concentration double (2 times) the film coverage for all solvents improved. When 2-ME employed to prepare the perovskite solution the perovskite grain size increased, number of voids decreased substantially (Figure 1d). We didn't observe significant morphology improvement when the perovskite concentration doubles and prepared with DMF solvent (Figure 1e). Surprisingly, homogenous pinhole free perovskite morphology is achieved when the perovskite precursor concentration doubles and prepared by DMAc solvent (Figure 1f). We concluded that high concentration perovskite dissolve in DMAc is suitable to produce highly uniform and homogenous perovskite film without antisolvent.

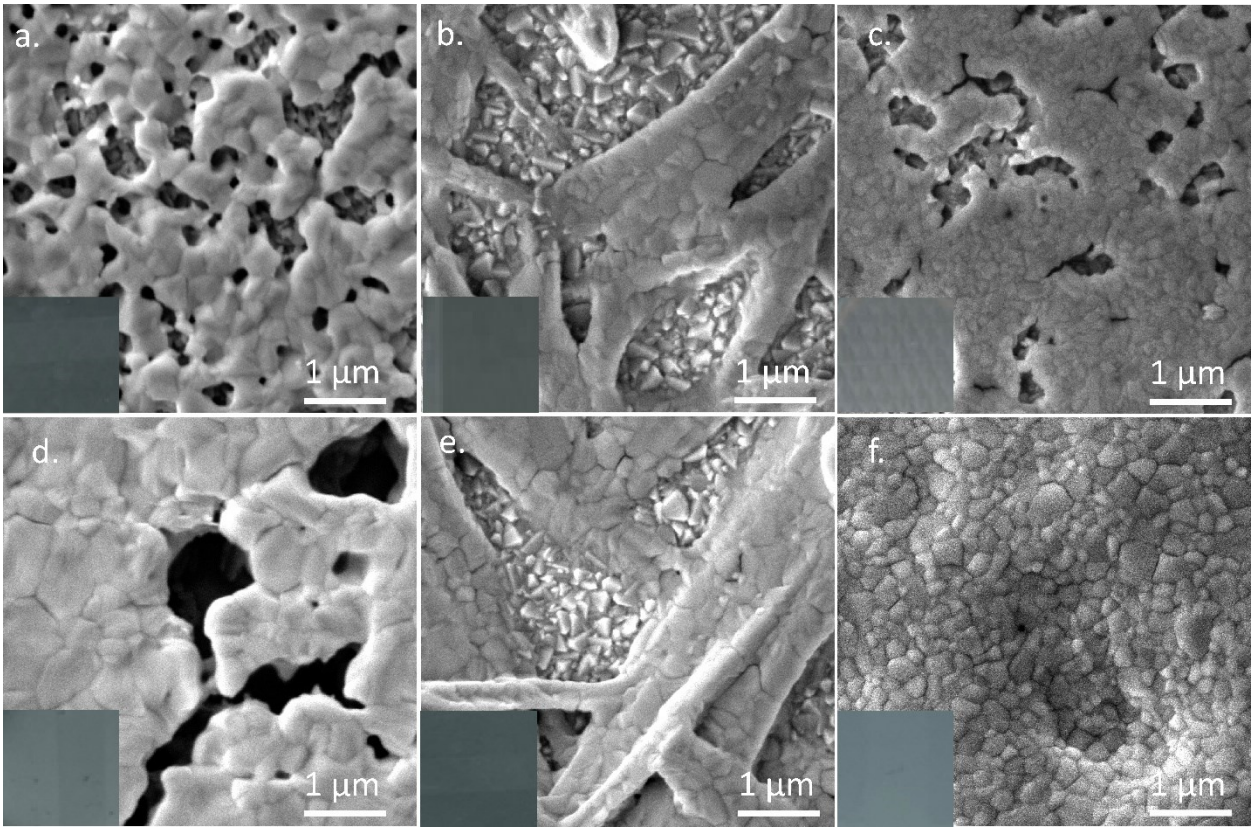

Figure 1. the surface SEM images of different concentration prepared perovskite films based on 2ME, DMF and DMAc precursor solution. a. 1 times 2ME; b. 1 times DMF; c. 1 times DMAc; d. 2 times 2ME; e. 2 times DMF; f. 2 times DMAc.

UV-vis and XRD of the perovskite films were using to further investigate the property of these films prepared from different solvents. The UV-vis of perovskite films prepared from 2-ME, DMF and DMAc 1 times and 2 times are presented in Figure S2. The absorption onset of the perovskite did not change due to the solvents. Obviously, the low concentration-based perovskite absorption intensity is weak, and when the precursor concentration doubled (2 times) the absorption of perovskite increased when 2-ME and DMAc were employed to prepare the perovskite precursor which is related with the formation of dense layer. However, 1 times and 2 times DMF based perovskite layer didn't exhibited absorption intensity shift in both cases the morphology continues significant voids. Furthermore, in the 2 times 2-ME and DMF based- films the UV-vis spectra baseline is much higher than the low perovskite concentration-based films which indicated the formation of very rough surface. Interestingly, even in high concentration, DMAc prepared perovskite UV-vis baseline in a lower intensity, which implied smooth perovskite morphology is formed by the DMAc-based perovskite precursor. As a result, the 2 times DMAc film produced a high-quality smooth and pinhole free perovskite film. Thus, from Figure S3 could see that the low concentration DMF-solvent based perovskite film we have observed the intermediate peak still remained after annealing 100 ºC for 30 min, however, for 2 times DMF-based films, the intermediate peaks completely disappear which is related with when the perovskite concentration increase, the proportion of the DMF reduced as a result solvent escape time decreased. For 2-ME prepared perovskite, both concentration films show PbI_2 peak around 12.9 degrees, but the corresponding as-prepared wet films showed in Figure S4 has no PbI_2 peak, which indicated that the pure 2-ME prepared perovskite films are not-thermally stable, and they could easily decompose during annealing. The 1 times DMAc film also has shown the PbI_2 peak, because the perovskite film is thin, MAI might decompose during annealing, however, when the

concentration of perovskite increased to 2 times, the PbI_2 peak completely disappeared. Then, turning to the element in the perovskite, in Figure S5a, the X-ray photoelectron spectroscopy (XPS) for these films. The peaks around 142 and 137 eV were assigned to $4f_{5/2}$ and $4f_{7/2}$ of divalent Pb^{2+}, respectively. The 2 times DMAc sample shift to higher binding energies at 142.5 and 137.7 eV, Figure S5b, I 3d peak around 630 and 618.5 eV were assigned to $3d_{3/2}$ and I $3d_{5/2}$, respectively, DMAc sample also have a red shift for all the peaks. The peaks shift of Pb 4f and I 3d to higher binding energy indicates that the perovskite has higher interaction with DMAc than DMF and 2ME.

4.2 Concentration effect on DMAc prepared perovskite films

We studied the influence of various concentrations of DMAc precursor-based perovskite film using UV-Vis and XRD (Figure 2a-b), Figure 2a showed the UV-vis absorption spectra of the and annealed (100 ºC for 30 min) perovskite films at different precursor concentration. All the perovskite films showed an absorption onset at 780 nm. The absorption coefficient, α, is calculated by the following formula:

$$\alpha = 2.303\frac{A}{t} \qquad \text{(equation 1)}$$

A is absorbance; t is thickness.[53] According to Figure S10, the thickness of 1 time and 2 times perovskite films are 100 nm and 600 nm, respectively. Then the α for 1 times perovskite film is $1.398*10^5$ cm^{-1}, and $5.0205*10^4$ cm^{-1} for 2 times perovskite film at 750 nm, which means most of incident light can be absorbed by both perovskite films, this is consistent with the literature report.[54-55] We also measured UV-Vis spectra and XRD for wet perovskite films prepared by different concentration precursor solutions (Figure S6a-b). The wet and annealed perovskite films showed similar features in our system, which is also shown in 2D GIWAXS patterns of 1 times

and 2 times DMAc based wet films (Figure S6 c-d). The film crystallinity for all concentrations improved when the perovskite film was annealed at 100 ºC which is evidenced with the ratio of perovskite peak at 14 degree and FTO glass peak at 26.3 degree of the respective layers (Figure S7). Intriguingly, a champion PCE of ~15% (Figure S8) was achieved using wet 2 times perovskite films perovskite films which demonstrated our system has a huge potential to fabricate antisolvent free and annealing free perovskite films. DLS was employed to study the size distribution of different concentration perovskite precursors (Figure S9), in which the peak around 5 nm is assigned to Pb-I individual octahedrons, the peak around 1000nm is assigned to the soft complex.[56] With the concentration increase, the peak around 5 nm slightly shifted to higher wavelength, which implies the colloid size in the precursor increased with increase in perovskite concentration.

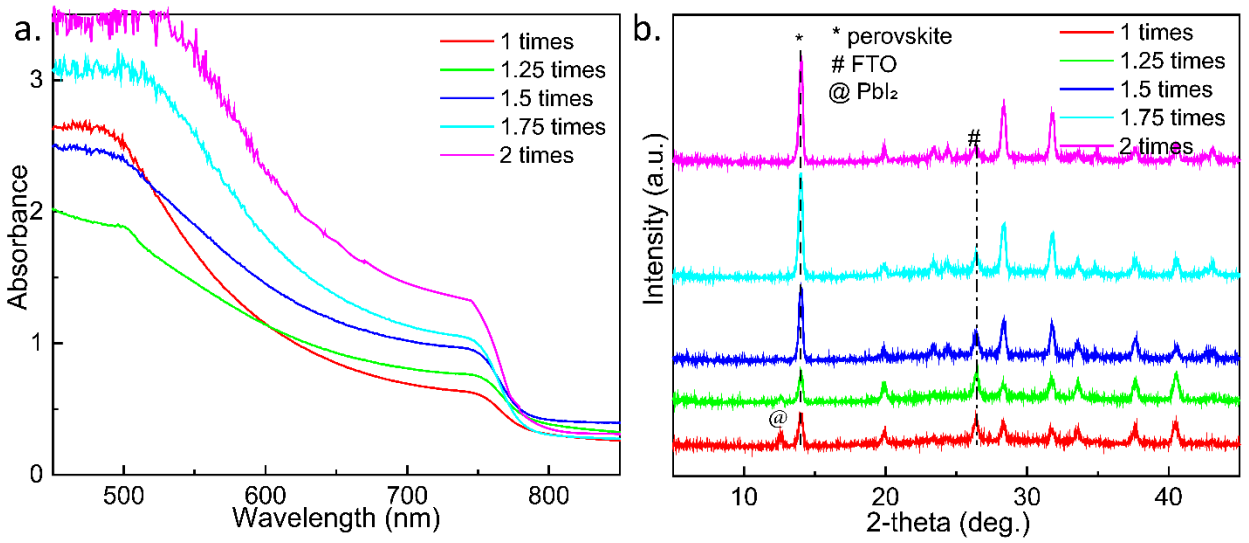

Figure 2. a. UV-vis absorption of the annealed (100 °C for 30 min) perovskite films which are prepared from DMAc solvent with different concentration. b. DMAc-based XRD patterns of the annealed films (100 °C and 30 min).

To study the influence of concentration and annealing on the evolution of perovskite morphology and coverage we recorded the top-view and cross-sectional SEM of various concentration DMAc prepared perovskite precursor-based films (Figure 3). Figure 3a-e and Figure

3f-j showed the as-prepared wet films and annealed films with a concentration of 1-, 1.25-, 1.5-, 1.75-, and 2 times, respectively. Figure 3a showed the top-view SEM of 1 times film, where several voids formed (less coverage). When the concentration increases to 1.25 times the coverage improves, however there are some spots shown in the perovskite layer (Figure 3b). For 1.5 times concentration we have observed the perovskite grain clearly without annealing, however, still there are voids present (Figure 3c). When the concentration further increases to 1.75- and 2 times, the

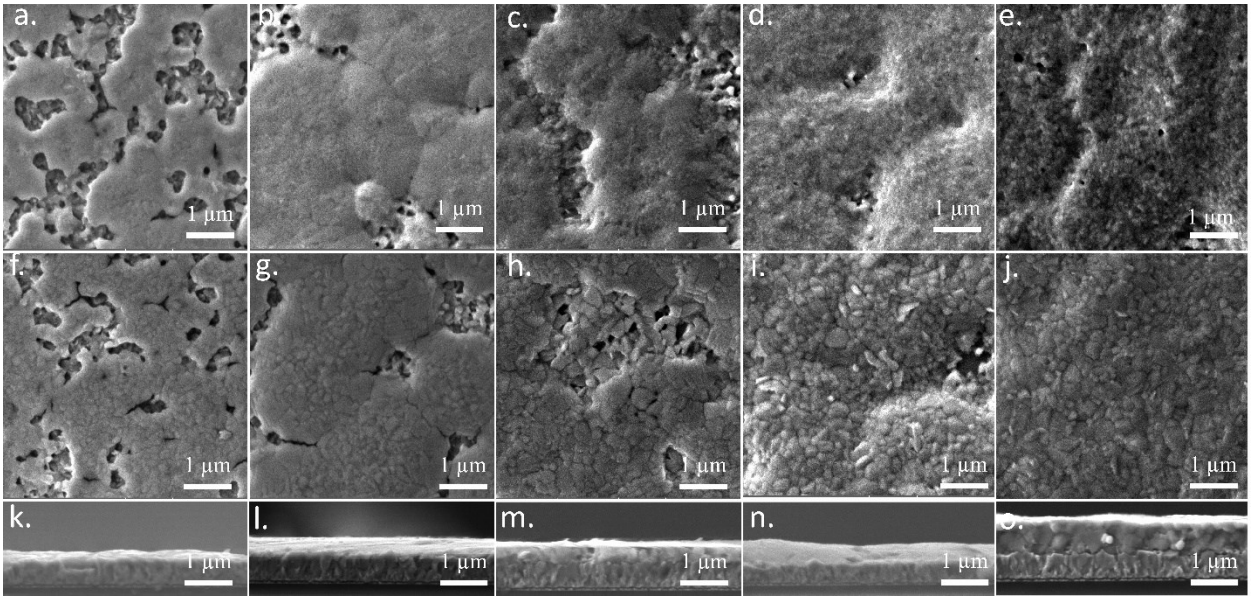

Figure 3.a-e. Wet films prepared by 1, 1.25, 1.5, 1.75- and 2-times perovskite precursor; f-j. Annealed perovskite films prepared by prepared by 1, 1.25, 1.5, 1.75- and 2-times perovskite precursor; k-o. Cross-section prepared by 1, 1.25, 1.5, 1.75- and 2-times perovskite precursor.

wet film coverage enhanced and several more perovskite grains formed before annealing, and at this stage the substrate is almost fully covered with perovskite. We provided a movie (Video S1-S5) that demonstrated the color change when various concentration DMAc-based perovskite precursors spin coated on the FTO. When the spin coating process started, the film color changed from colorless to white, yellow, brown, and finally black perovskite film formed. These color changes are similar for all concentrations, however, when the concentration increased, it took

longer time to turn black phase (slow evaporation) which indicates that high concentration perovskite precursor will induce perovskite crystallization to form high quality perovskite films. After annealing, the perovskite average grain size increases where the 1- and 1.25-times films (Figure 3f and 3g) exhibited about 50 nm average grain sizes, and when the concentration increase the average grain size increased as a result the 1.5-, 1.75- and 2-times films showed average grain

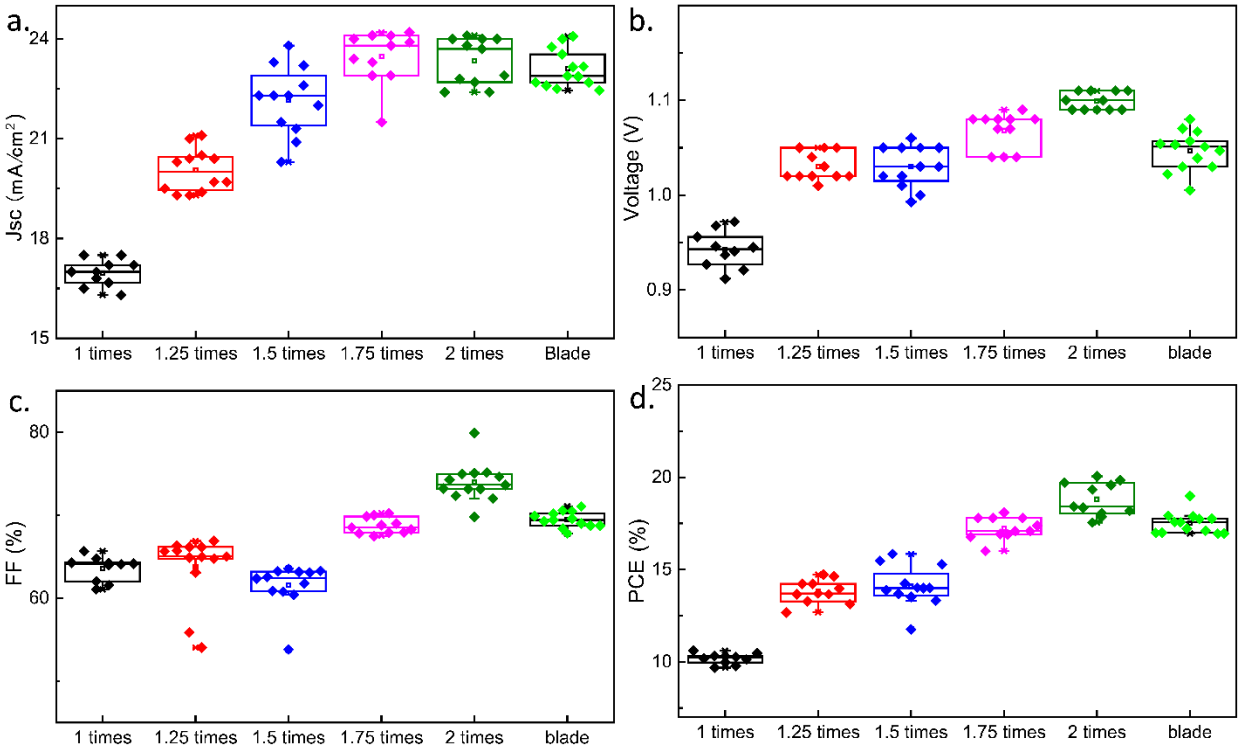

Figure 4. Statistics of photovoltaic parameters of PSCs by different perovskite precursor concentration and blade coated prepared 2 times devices. (a) J_{sc}; (b) V_{oc}; (c) FF, and (d) PCE.

size of about 400 nm. Especially the 2 times DMAc precursor produced homogenous compact perovskite films. Figure 3k-o showed the cross-sectional images for various concentrations discussed above. The 1 times film thickness is less than 100 nm, the 1.25 times film is slightly thicker than 1 times film. The 1.5 times film thickness is ~200 nm thickness, and pinholes observed in its cross section. The 2 times film thickness is about 600 nm and intriguingly the film also

compact in the cross-sectional image, which implies that high perovskite precursor concentration retards perovskite crystallization and improves the perovskite grain quality. Figure S10 showed the full SEM image of Figure 3k-o, the original SEM images show that all samples measured under 40.0 k.

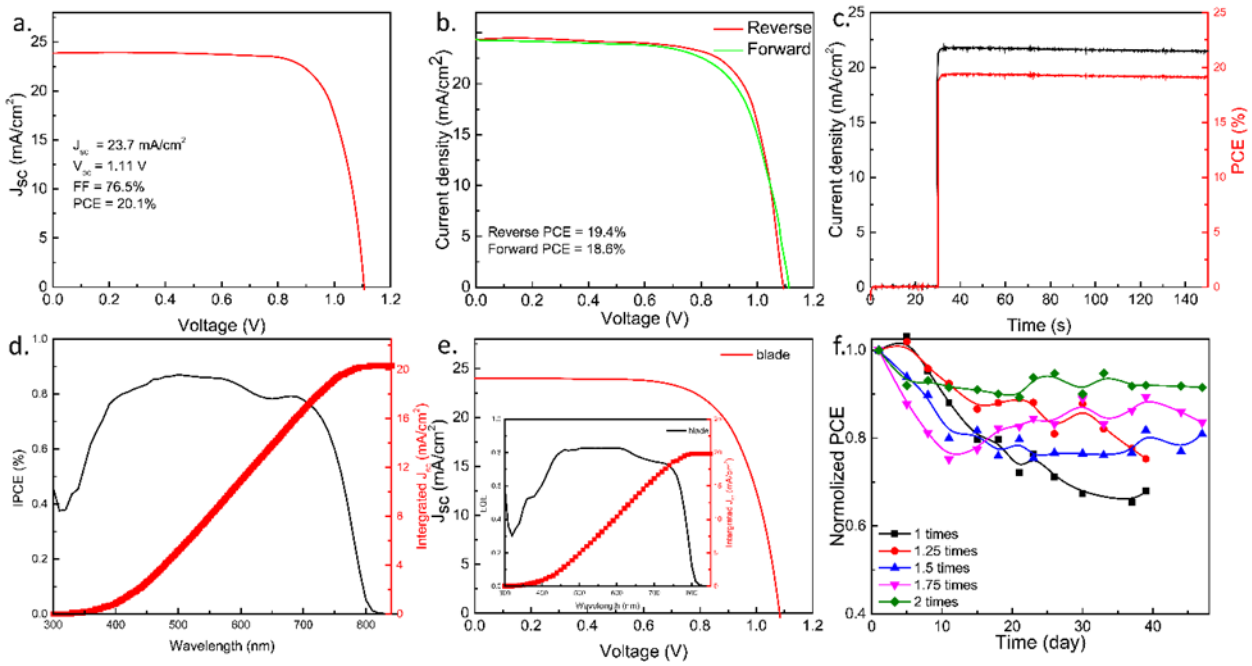

Figure 5. a. J-V curve of the optimized spin-coated device; b. Reverse and forward scan J-V curves of the 2 times spin coated-based perovskite PSCs; c. Stabilized power output of the best spin coated device; d. IPCE of the best spin coated device; e, J-V curve of the champion blade coated device. The inset in Figure 1e is the champion blade coated device IPCE, f. Long-term stability of different perovskite precursor concentration spin coated devices.

To assess the influence of various concentration of perovskite precursors in DMAc we fabricated a perovskite device with a structure of FTO/SnO_2/Perovskite/Spiro-OMeTAD/Au, we prepare the perovskite layer with spin-coating without anti-solvent and to demonstrate the potential of DMAc solvent-blade perovskite precursor for commercial application, we fabricated a perovskite using blade-coater. The photovoltaic parameters are summarized in box chart in Figure 4. Figure 4a showed the short-circuit current density (J_{sc}), where the J_{sc} increased with increase in

concentration. Blade-coated perovskite demonstrated the highest J_{sc} compared to the spin-coated films attributed to its dense thickness. The open-circuit voltage (V_{oc}) and fill factor (FF) showed similar trends with the J_{sc} (Figure 4b and 4c) when the concentration increase both V_{oc} and FF improved. However, the blades coated perovskite exhibited slightly lower V_{oc} and FF than the spin coated 2 times-based devices. Figure 4d showed the PCE of the devices fabricated, where the average PCE 10%, 14.5%, 14.6%, 17.8%, 19% were achieved for 1-, 1.25-, 1.5-, 1.75-, and 2 times perovskite concentrations, respectively. Unfortunately, we fabricate PSCs at RH>40%, and the PCE only reach 10% (Figure S11), because too much water will break the hydrogen bonds between PbI_2 and CH_3NH_3I.[57] We prepared large area perovskite film (1.5 ×10 cm^2) by blade coater (Figure S12) and cut to 1.5 ×1.5 cm^2 to fit our mask size to assess the device performance, where surprisingly our blade-coated device exhibited an average PCE of 17.5%. We have also fabricated devices using 2-ME and DMF using the low (1 times) and high (2 times) concentration and the results are presented in Figure S13. However, the devices from both solvents exhibited poor performance (PCE= ~5%), when the concentration increases the photovoltaic parameters showed improvements.

Figure 5a showed the champion devices J-V curve prepared by 2 times perovskite precursor, where a maximum PCE of 20.1% with a V_{oc} of 1.11 V, FF of 76.5%, and J_{sc} of 23.7 mA/cm^2 achieved, with non-significant difference in the performance of the device when measured from reverse and forward scan directions 19.4% PCE vs 18.6% PCE, respectively (Figure 5b). Furthermore, the device demonstrated stable power output of 19.1% at 0.89 V bias (Figure 5c). To verify the J_{sc} measured in the J-V measurement we have recorded the external quantum efficiency (EQE) of the device again and presented the data in Figure 5d, where we have observed that high EQE intensity of over 0.8 achieved in the range of 450-650 nm with an integrated J_{sc} of 20.4

mA/cm^2. The calculated J_{sc} is 14% discrepancy with the J_{sc} measured in the J-V curve which is acceptable.[58] In the EQE measurement, the external bias leads to ion migration inside the perovskite film.[58] Moreover, in the EQE measurement a single wavelength with much lower intensity than the one sun radiation is used.[44, 59] Additionally, the perovskite device could degrade under long-term light irradiation during IPCE measurement, these all made the difference in J_{sc} measured from J-V and EQE.[58] Furthermore, we studied the stability of the unencapsulated spin coated devices in air (RH = ~20%, and T=30ºC) for 47 days, where the device fabricated with 2 times DMAc system maintained more than 90% of its initial value, which displayed that DMAc is a very suitable solvent to widely use.

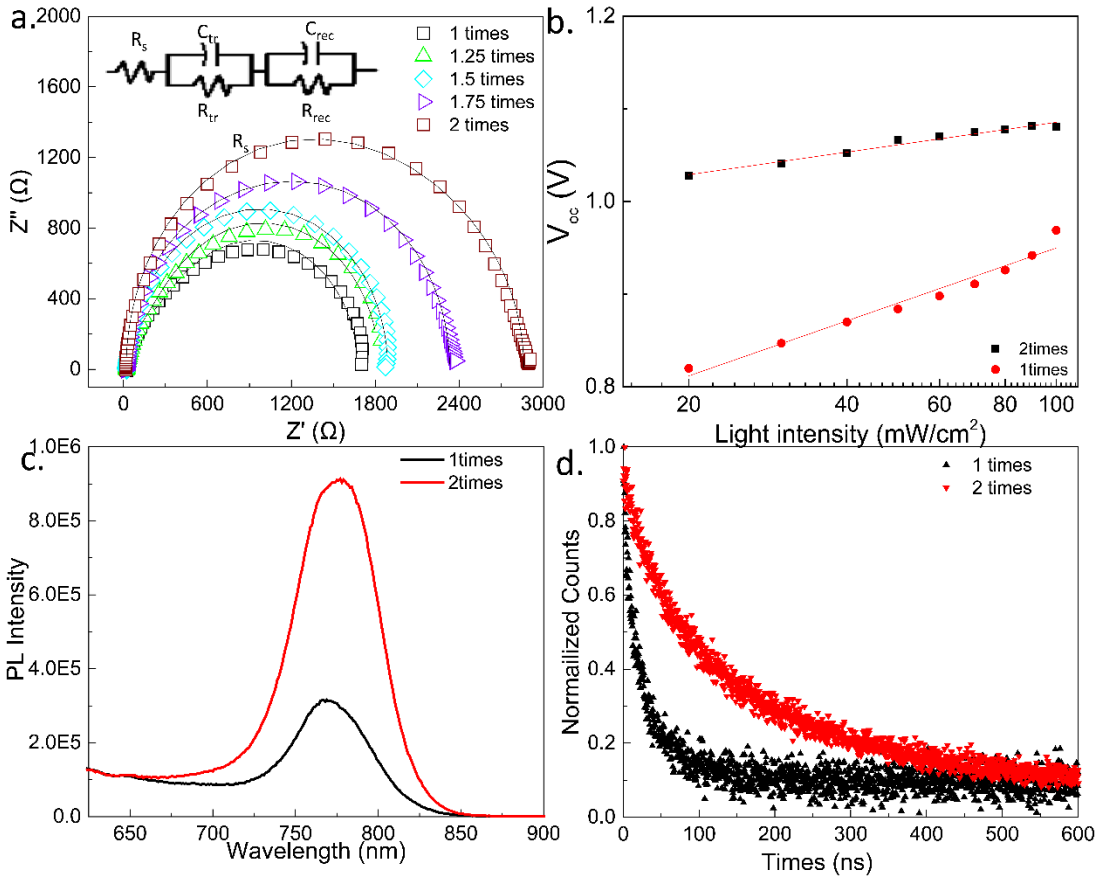

Figure 6. a. Electrochemical impedance spectra curve of various perovskite precursor concentration-based PSCs; b. V_{oc} as a function of incident light intensity; c. PL of glass/perovskite/ spiro-OMeTAD for different concentration perovskite layers. d. TRPL glass/perovskite/ spiro-OMeTAD for different concentration perovskite layers.

Figure 6 exhibited the effect of perovskite precursor concentration on the optoelectronic properties. Figure 6a showed the Nyquist plot of the devices based on different perovskite precursor concentration under dark conditions. The EIS fitting parameters are summarized in Table S1, the R_s is series residences, which is mainly contributed to the sheet resistance of FTO glass according to the literature.[60]. The variation of R_s values is attributed to different batches of FTO, and our R_s values are still in the reasonable range of the reported R_s values.[60-64] Therefore, we do not think the Rs first decreases and then increases as the concentration increases. R_{tr} is the charge transfer resistance and R_{rec} is the recombination resistance. The 2 times device has the smallest R_s of 19.02 Ω, smallest R_{tr} 76.7 Ω, and the largest R_{rec} of 2774 Ω. The decrease in R_{tr} for the 2-times signified for the better interfacial charge transport behavior. Moreover, the increase in R_{rec} made the charge recombination in the 2-times based device difficult, which confirms that the charge recombination loss is significantly suppressed in the high concentration perovskite precursor. Figure 6b showed the ideality factor plot which is extracted from the V_{oc} vs illumination plot by calculating the slope in the linear regions following equation 1, where n is the ideality factor, q is the elementary charge, K is the Boltzmann constant, and T is the thermodynamic temperature. The 2 times device showed n = 3.11, whereas the 1 n increased to 7.6 for the 1 times device, which suggested that the trap-assisted non-radiative recombination is suppressed in 2 times device compared to the 1 times device.

$$n = \frac{q}{KT}\frac{dVoc}{dln(I)} \qquad \text{equation (2)}$$

Figure S13 showed the typical dark current-voltage characteristic curves of electron-only devices

prepared by 2times DMAc. The number of defects is calculated by the following equation:

$$N_{traps} = \frac{2\varepsilon\varepsilon_0 V_{TFL}}{eL^2} \quad \text{equation (3)}$$

The ε is the relative dielectric constant, ε_0 is vacuum permittivity, V_{TFL} is trap filled limit voltage, e is the elementary charge, and L is the thickness of perovskite films. The calculated N_{traps} for the 2 times DMAc prepared devices exhibited $1.621*10^{16}cm^{-3}$. Figure 6c showed the steady-state PL spectra of the different concentration perovskite films, where the 2 times perovskite film exhibited higher PL intensity than 1 times perovskite which implied in the 2 times perovskite layer had less charge recombination observed than the 1 times perovskite. The TRPL data of these films are shown in Figure 6d. The lifetime value of 2 times perovskite film is 217 ns, which is 4 times longer than 1 times perovskite film, the TRPL curves are fitted by the bi-exponential decay function and the fitting parameters are summarized in Table S2.

5. Conclusion

In this work, we developed the preparation of anti-solvent free $MAPbI_3$ using DMAc solvent. We studied morphology evolution and perovskite crystal growth of $MAPbI_3$ in different solvents by vary the concentration. We found that the 2 times (2.12mM) perovskite concentration in DMAc produced homogenous and compact perovskite films while spun without anti-solvent in air. As a result, devices fabricated with such perovskite produced an outstanding PCE of 20.1% and 18% PCE for the spin coated and blade coated prepared perovskite films, respectively. This work stablished an alternative solvent system to fabricate high performance and stable device in air and without the need of anti-solvent, which influenced the reproducibility of the devices as well as adding extra cost.

Declaration of competing interest

The authors declare that they have no known competing financial interests or personal relationships that could have appeared to influence the work reported in this paper.

Data availability

Data will be made available on request.

ACKNOWLEDGMENT

Q. D. and Y. Q thank National Science Foundation (DMR- 2242467) for the providing financial support. Q. Z. is supported by NSF-PREM grant #DMR-1826886. The steady-state PL and TRPL equipment used in this work is supported by National Science Foundation Research Initiation Award: Novel Perovskite Solar Cells Based on Interface Manipulation (Award#1900047). G. M. and X.G. thank NSF grant OIA-1757220 for providing financial support for 2D GIWAXS measurements. Jada Emodogo supported is by the National Science Foundation under Grant No. OIA-2225852. D.L. acknowledges partial support from NSF ECCS #2053954 for the SEM measurements.

Reference

1. Tang, H.; He, S.; Peng, C., A short progress report on high-efficiency perovskite solar cells. *Nanoscale research letters* **2017,** *12* (1), 1-8.

2. Fu, R.; Zhou, W.; Li, Q.; Zhao, Y.; Yu, D.; Zhao, Q., Stability challenges for perovskite solar cells. *ChemNanoMat* **2019,** *5* (3), 253-265.
3. Chen, W.; Wu, Y.; Yue, Y.; Liu, J.; Zhang, W.; Yang, X.; Chen, H.; Bi, E.; Ashraful, I.; Grätzel, M., Efficient and stable large-area perovskite solar cells with inorganic charge extraction layers. *Science* **2015,** *350* (6263), 944-948.
4. Green, M. A.; Ho-Baillie, A.; Snaith, H. J., The emergence of perovskite solar cells. *Nature photonics* **2014,** *8* (7), 506-514.
5. Laban, W. A.; Etgar, L., Depleted hole conductor-free lead halide iodide heterojunction solar cells. *Energy & Environmental Science* **2013,** *6* (11), 3249-3253.
6. Dong, Q.; Fang, Y.; Shao, Y.; Mulligan, P.; Qiu, J.; Cao, L.; Huang, J., Electron-hole diffusion lengths> 175 μm in solution-grown $CH_3NH_3PbI_3$ single crystals. *Science* **2015,** *347* (6225), 967-970.
7. Xing, G.; Mathews, N.; Sun, S.; Lim, S. S.; Lam, Y. M.; Grätzel, M.; Mhaisalkar, S.; Sum, T. C., Long-range balanced electron-and hole-transport lengths in organic-inorganic $CH_3NH_3PbI_3$. *Science* **2013,** *342* (6156), 344-347.
8. Stranks, S. D.; Eperon, G. E.; Grancini, G.; Menelaou, C.; Alcocer, M. J.; Leijtens, T.; Herz, L. M.; Petrozza, A.; Snaith, H. J., Electron-hole diffusion lengths exceeding 1 micrometer in an organometal trihalide perovskite absorber. *Science* **2013,** *342* (6156), 341-344.
9. Yoo, J. J.; Seo, G.; Chua, M. R.; Park, T. G.; Lu, Y.; Rotermund, F.; Kim, Y.-K.; Moon, C. S.; Jeon, N. J.; Correa-Baena, J.-P., Efficient perovskite solar cells via improved carrier management. *Nature* **2021,** *590* (7847), 587-593.
10. Kim, M.; Jeong, J.; Lu, H.; Lee, T. K.; Eickemeyer, F. T.; Liu, Y.; Choi, I. W.; Choi, S. J.; Jo, Y.; Kim, H.-B., Conformal quantum dot–SnO_2 layers as electron transporters for efficient perovskite solar cells. *Science* **2022,** *375* (6578), 302-306.
11. Chu, L.; Zhai, S.; Ahmad, W.; Zhang, J.; Zang, Y.; Yan, W.; Li, Y., High-performance large-area perovskite photovoltaic modules. *Nano Research Energy* **2022,** *1* (2), e9120024.
12. Wang, M.; Cao, F.; Deng, K.; Li, L., Adduct phases induced controlled crystallization for mixed-cation perovskite solar cells with efficiency over 21%. *Nano Energy* **2019,** *63*, 103867.
13. Tumen-Ulzii, G.; Qin, C.; Klotz, D.; Leyden, M. R.; Wang, P.; Auffray, M.; Fujihara, T.; Matsushima, T.; Lee, J. W.; Lee, S. J., Detrimental effect of unreacted PbI_2 on the long-term stability of perovskite solar cells. *Advanced Materials* **2020,** *32* (16), 1905035.
14. Shi, P.; Ding, Y.; Ren, Y.; Shi, X.; Arain, Z.; Liu, C.; Liu, X.; Cai, M.; Cao, G.; Nazeeruddin, M. K., Template-Assisted Formation of High-Quality α-Phase $HC(NH_2)_2PbI_3$ Perovskite Solar Cells. *Advanced Science* **2019,** *6* (21), 1901591.
15. Fang, Z.; Wang, L.; Mu, X.; Chen, B.; Xiong, Q.; Wang, W. D.; Ding, J.; Gao, P.; Wu, Y.; Cao, J., Grain boundary engineering with self-assembled porphyrin supramolecules for highly efficient large-area perovskite photovoltaics. *Journal of the American Chemical Society* **2021,** *143* (45), 18989-18996.
16. Wang, X.; Fan, Y.; Wang, L.; Chen, C.; Li, Z.; Liu, R.; Meng, H.; Shao, Z.; Du, X.; Zhang, H., Perovskite solution aging: what happened and how to inhibit? *Chem* **2020,** *6* (6), 1369-1378.
17. Zhang, Y.; Chen, M.; Zhou, Y.; Li, W.; Lee, Y.; Kanda, H.; Gao, X. X.; Hu, R.; Brooks, K. G.; Zia, R., The Synergism of DMSO and Diethyl Ether for Highly Reproducible and Efficient $MA_{0.5}FA_{0.5}PbI_3$ Perovskite Solar Cells. *Advanced Energy Materials* **2020,** *10* (29), 2001300.
18. Wang, H.; Zeng, W.; Xia, R., Antisolvent diethyl ether as additive to enhance the performance of perovskite solar cells. *Thin Solid Films* **2018,** *663*, 9-13.

19. Zhang, W.; Li, Y.; Liu, X.; Tang, D.; Li, X.; Yuan, X., Ethyl acetate green antisolvent process for high-performance planar low-temperature SnO_2-based perovskite solar cells made in ambient air. *Chemical Engineering Journal* **2020,** *379*, 122298.
20. Bu, T.; Wu, L.; Liu, X.; Yang, X.; Zhou, P.; Yu, X.; Qin, T.; Shi, J.; Wang, S.; Li, S., Synergic interface optimization with green solvent engineering in mixed perovskite solar cells. *Advanced Energy Materials* **2017,** *7* (20), 1700576.
21. Ueoka, N.; Oku, T.; Suzuki, A., Effects of doping with Na, K, Rb, and formamidinium cations on $(CH_3NH_3)_{0.99}Rb_{0.01}Pb_{0.99}Cu_{0.01}I3_{-x}(Cl, Br)_x$ perovskite photovoltaic cells. *AIP Advances* **2020,** *10* (12), 125023.
22. Bai, X.; Zou, X.; Zhu, J.; Pei, Y.; Yang, Y.; Jin, W.; Chen, D., Effect of Rb doping on modulating grain shape and semiconductor properties of $MAPbI_3$ perovskite layer. *Materials Letters* **2018,** *211*, 328-330.
23. Bella, F.; Renzi, P.; Cavallo, C.; Gerbaldi, C., Caesium for perovskite solar cells: an overview. *Chemistry–A European Journal* **2018,** *24* (47), 12183-12205.
24. Zhang, X.; Ren, X.; Liu, B.; Munir, R.; Zhu, X.; Yang, D.; Li, J.; Liu, Y.; Smilgies, D.-M.; Li, R., Stable high efficiency two-dimensional perovskite solar cells via cesium doping. *Energy & Environmental Science* **2017,** *10* (10), 2095-2102.
25. Sabba, D.; Mulmudi, H. K.; Prabhakar, R. R.; Krishnamoorthy, T.; Baikie, T.; Boix, P. P.; Mhaisalkar, S.; Mathews, N., Impact of anionic Br–substitution on open circuit voltage in lead free perovskite ($CsSnI_{3-x}Br_x$) solar cells. *The journal of physical chemistry C* **2015,** *119* (4), 1763-1767.
26. Zhang, H.; Lv, Y.; Wang, J.; Ma, H.; Sun, Z.; Huang, W., Influence of Cl incorporation in perovskite precursor on the crystal growth and storage stability of perovskite solar cells. *ACS applied materials & interfaces* **2019,** *11* (6), 6022-6030.
27. Son, D.-Y.; Lee, J.-W.; Choi, Y. J.; Jang, I.-H.; Lee, S.; Yoo, P. J.; Shin, H.; Ahn, N.; Choi, M.; Kim, D., Self-formed grain boundary healing layer for highly efficient $CH_3NH_3PbI_3$ perovskite solar cells. *Nature Energy* **2016,** *1* (7), 1-8.
28. Ma, F.; Li, J.; Li, W.; Lin, N.; Wang, L.; Qiao, J., Stable α/δ phase junction of formamidinium lead iodide perovskites for enhanced near-infrared emission. *Chemical science* **2017,** *8* (1), 800-805.
29. Hendriks, K. H.; van Franeker, J. J.; Bruijnaers, B. J.; Anta, J. A.; Wienk, M. M.; Janssen, R. A., 2-Methoxyethanol as a new solvent for processing methylammonium lead halide perovskite solar cells. *Journal of Materials Chemistry A* **2017,** *5* (5), 2346-2354.
30. Deng, W.; Li, F.; Li, J.; Wang, M.; Hu, Y.; Liu, M., Anti-solvent free fabrication of FA-Based perovskite at low temperature towards to high performance flexible perovskite solar cells. *Nano Energy* **2020,** *70*, 104505.
31. Yang, W.; Zhan, Y.; Yang, F.; Li, Y., Hot-Casting and Anti-solvent Free Fabrication of Efficient and Stable Two-Dimensional Ruddlesden–Popper Perovskite Solar Cells. *ACS Applied Materials & Interfaces* **2021,** *13* (51), 61039-61046.
32. Chen, H.; Ding, X.; Xu, P.; Hayat, T.; Alsaedi, A.; Yao, J.; Ding, Y.; Dai, S., Forming intermediate phase on the surface of PbI2 precursor films by short-time DMSO treatment for high-efficiency planar perovskite solar cells via vapor-assisted solution process. *ACS applied materials & interfaces* **2018,** *10* (2), 1781-1791.
33. Wei, Z.; Chen, H.; Yan, K.; Yang, S., Inkjet printing and instant chemical transformation of a $CH_3NH_3PbI_3$/nanocarbon electrode and interface for planar perovskite solar cells. *Angewandte Chemie International Edition* **2014,** *53* (48), 13239-13243.

34. Noel, N. K.; Habisreutinger, S. N.; Wenger, B.; Klug, M. T.; Hörantner, M. T.; Johnston, M. B.; Nicholas, R. J.; Moore, D. T.; Snaith, H. J., A low viscosity, low boiling point, clean solvent system for the rapid crystallisation of highly specular perovskite films. *Energy & Environmental Science* **2017,** *10* (1), 145-152.
35. Lv, M.; Dong, X.; Fang, X.; Lin, B.; Zhang, S.; Ding, J.; Yuan, N., A promising alternative solvent of perovskite to induce rapid crystallization for high-efficiency photovoltaic devices. *RSC Advances* **2015,** *5* (26), 20521-20529.
36. Chen, A. Z.; Shiu, M.; Deng, X.; Mahmoud, M.; Zhang, D.; Foley, B. J.; Lee, S.-H.; Giri, G.; Choi, J. J., Understanding the formation of vertical orientation in two-dimensional metal halide perovskite thin films. *Chemistry of Materials* **2019,** *31* (4), 1336-1343.
37. Chen, A. Z.; Shiu, M.; Ma, J. H.; Alpert, M. R.; Zhang, D.; Foley, B. J.; Smilgies, D.-M.; Lee, S.-H.; Choi, J. J., Origin of vertical orientation in two-dimensional metal halide perovskites and its effect on photovoltaic performance. *Nature communications* **2018,** *9* (1), 1-7.
38. Zhang, X.; Fei, C.; Shen, L.; Baral, P.; Vijayaraghavan, S. N.; Yan, F.; Gong, X.; Wang, H., Manipulating Nucleation and Crystal Growth of Inorganic Perovskite Solar Cells. *ACS Applied Materials & Interfaces* **2023,** *15* (32), 38522-38529.
39. Chao, L.; Xia, Y.; Duan, X.; Wang, Y.; Ran, C.; Niu, T.; Gu, L.; Li, D.; Hu, J.; Gao, X., Direct and stable α-phase formation via ionic liquid solvation for formamidinium-based perovskite solar cells. *Joule* **2022,** *6* (9), 2203-2217.
40. Fu, R.; Zhao, Y.; Zhou, W.; Li, Q.; Zhao, Y.; Zhao, Q., Ultrahigh open-circuit voltage for high performance mixed-cation perovskite solar cells using acetate anions. *Journal of Materials Chemistry A* **2018,** *6* (29), 14387-14391.
41. Gao, C.; Dong, H.; Bao, X.; Zhang, Y.; Saparbaev, A.; Yu, L.; Wen, S.; Yang, R.; Dong, L., Additive engineering to improve the efficiency and stability of inverted planar perovskite solar cells. *Journal of Materials Chemistry C* **2018,** *6* (30), 8234-8241.
42. Xie, J.; Zhou, Z.; Qiao, H.; Chen, M.; Wang, L.; Yang, S.; Hou, Y.; Yang, H., Modulating $MAPbI_3$ perovskite solar cells by amide molecules: Crystallographic regulation and surface passivation. *Journal of Energy Chemistry* **2021,** *56*, 179-185.
43. Zhang, Q.; Ma, G.; Green, K. A.; Gollinger, K.; Moore, J.; Demeritte, T.; Ray, P. C.; Hill Jr, G. A.; Gu, X.; Morgan, S. E., $FAPbI_3$ perovskite films prepared by solvent self-volatilization for photovoltaic applications. *ACS Applied Energy Materials* **2022,** *5* (2), 1487-1495.
44. Abate, S. Y.; Zhang, Q.; Qi, Y.; Nash, J.; Gollinger, K.; Zhu, X.; Han, F.; Pradhan, N.; Dai, Q., Universal Surface Passivation of Organic–Inorganic Halide Perovskite Films by Tetraoctylammonium Chloride for High-Performance and Stable Perovskite Solar Cells. *ACS Applied Materials & Interfaces* **2022,** *14* (24), 28044-28059.
45. Qi, Y.; Almtiri, M.; Giri, H.; Jha, S.; Ma, G.; Shaik, A. K.; Zhang, Q.; Pradhan, N.; Gu, X.; Hammer, N. I., Evaluation of the passivation effects of PEDOT: PSS on inverted perovskite solar cells. *Advanced Energy Materials* **2022,** *12* (46), 2202713.
46. Singh, T.; Miyasaka, T., Stabilizing the efficiency beyond 20% with a mixed cation perovskite solar cell fabricated in ambient air under controlled humidity. *Advanced Energy Materials* **2018,** *8* (3), 1700677.
47. Li, H.; Bu, T.; Li, J.; Lin, Z.; Pan, J.; Li, Q.; Zhang, X.-L.; Ku, Z.; Cheng, Y.-B.; Huang, F., Ink engineering for blade coating FA-dominated perovskites in ambient air for efficient solar cells and modules. *ACS Applied Materials & Interfaces* **2021,** *13* (16), 18724-18732.

48. Meng, L.; Wei, Q.; Yang, Z.; Yang, D.; Feng, J.; Ren, X.; Liu, Y.; Liu, S. F., Improved perovskite solar cell efficiency by tuning the colloidal size and free ion concentration in precursor solution using formic acid additive. *Journal of Energy Chemistry* **2020,** *41*, 43-51.
49. Hamill Jr, J. C.; Schwartz, J.; Loo, Y.-L., Influence of solvent coordination on hybrid organic–inorganic perovskite formation. *ACS Energy Letters* **2017,** *3* (1), 92-97.
50. Chao, L.; Niu, T.; Gao, W.; Ran, C.; Song, L.; Chen, Y.; Huang, W., Solvent engineering of the precursor solution toward large-area production of perovskite solar cells. *Advanced Materials* **2021,** *33* (14), 2005410.
51. Kim, J.; Park, B.-w.; Baek, J.; Yun, J. S.; Kwon, H.-W.; Seidel, J.; Min, H.; Coelho, S.; Lim, S.; Huang, S., Unveiling the relationship between the perovskite precursor solution and the resulting device performance. *Journal of the American Chemical Society* **2020,** *142* (13), 6251-6260.
52. Di Girolamo, D.; Pascual, J.; Aldamasy, M. H.; Iqbal, Z.; Li, G.; Radicchi, E.; Li, M.; Turren-Cruz, S.-H.; Nasti, G.; Dallmann, A., Solvents for processing stable tin halide perovskites. *ACS Energy Letters* **2021,** *6* (3), 959-968.
53. Rai, R.; Singh, B. In *Absorbance and transmittance measurement of CsI thin films*, DAE-BRNS symposium on nuclear physics. V. 58, 2013.
54. Wu, J.; Chen, J.; Wang, H., Phase Transition Kinetics of $MAPbI_3$ for Tetragonal-to-Orthorhombic Evolution. *JACS Au* **2023,** *3* (4), 1205-1212.
55. Zhao, J.; Li, J.; Liu, X.; Bannenberg, L. J.; Bruno, A.; Savenije, T. J., Charge Carrier Dynamics in Co-evaporated $MAPbI_3$ with a Gradient in Composition. *ACS Applied Energy Materials* **2022,** *5* (6), 7049-7055.
56. Boonmongkolras, P.; Kim, D.; Alhabshi, E. M.; Gereige, I.; Shin, B., Understanding effects of precursor solution aging in triple cation lead perovskite. *RSC advances* **2018,** *8* (38), 21551-21557.
57. Dong, X.; Fang, X.; Lv, M.; Lin, B.; Zhang, S.; Ding, J.; Yuan, N., Improvement of the humidity stability of organic–inorganic perovskite solar cells using ultrathin Al_2O_3 layers prepared by atomic layer deposition. *Journal of Materials Chemistry A* **2015,** *3* (10), 5360-5367.
58. Saliba, M.; Etgar, L., Current density mismatch in perovskite solar cells. *ACS Energy Letters* **2020,** *5* (9), 2886-2888.
59. Yella, A.; Lee, H.; Tsao, H.; Yi, C.; Chandiran, A., Porphyrin-sensitized solar cells with cobalt (II/III)-based redox electrolyte exceed 12 percent efficiency (vol 334, pg 629, 2011). *Science* **2011,** *334* (6060), 1203-1203.
60. Pham, N. D.; Tiong, V. T.; Chen, P.; Wang, L.; Wilson, G. J.; Bell, J.; Wang, H., Enhanced perovskite electronic properties via a modified lead (ii) chloride Lewis acid–base adduct and their effect in high-efficiency perovskite solar cells. *Journal of Materials Chemistry A* **2017,** *5* (10), 5195-5203.
61. Liu, H.; Fu, X.; Fu, W.; Zong, B.; Huang, L.; Bala, H.; Wang, S.; Guo, Z.; Sun, G.; Cao, J., An effective TiO_2 blocking layer for hole-conductor-free perovskite solar cells based on carbon counter electrode. *Organic Electronics* **2018,** *59*, 253-259.
62. Jiang, P.; Xiong, Y.; Xu, M.; Mei, A.; Sheng, Y.; Hong, L.; Jones, T. W.; Wilson, G. J.; Xiong, S.; Li, D., The influence of the work function of hybrid carbon electrodes on printable mesoscopic perovskite solar cells. *The Journal of Physical Chemistry C* **2018,** *122* (29), 16481-16487.
63. Zhao, J.; Zhang, Y.; Zhao, X.; Zhang, J.; Wang, H.; Zhu, Z.; Liu, Q., Band alignment strategy for printable triple mesoscopic perovskite solar cells with enhanced photovoltage. *ACS Applied Energy Materials* **2019,** *2* (3), 2034-2042.

64. Zhang, Z.-L.; Li, J.-F.; Wang, X.-L.; Qin, J.-Q.; Shi, W.-J.; Liu, Y.-F.; Gao, H.-P.; Mao, Y.-L., Enhancement of perovskite solar cells efficiency using N-doped TiO 2 nanorod arrays as electron transfer layer. *Nanoscale Research Letters* **2017,** *12*, 1-7.